Numerical Study on RF-Induced Power Deposition of Cardiac Stents at 5T MRI

Ao Shen, Mir Khadiza Akter, Jianfeng Zheng, Ji Chen

Department of Electrical and Computer Engineering, University of Houston

Abstract

The U.S. Food and Drug Administration (FDA) has recently approved the 5T whole-body MRI system for clinical use. However, its distinct electromagnetic field distribution and shorter resonant wavelength introduce potential safety risks for patients with implants.

This study investigates RF-induced heating near stents of varying lengths placed in the right common carotid artery during 5T MRI using FDTD-based simulations (Sim4Life v7.2). Stents (20–60 mm in length, 4 mm in diameter) were positioned in anatomically realistic male and female models inside a 16-port circularly polarized RF coil operating at 210.8 MHz. Results were normalized according to the 2 W/kg whole-body and 3.2 W/kg head SAR limits, to evaluate 1g-averaged SAR near the stents and the 30-minute temperature rise for the worst-case scenario.

SAR consistently peaked at the stent edges, with the highest values occurring at the isocentre. For male models, SAR increased from 12.8 W/kg (20 mm) to 72.9 W/kg (60 mm), and for female models, from 27.2 W/kg to 87.3 W/kg, approaching half-wavelength resonance. Despite these elevated local SAR values, the maximum temperature rise remained below 1 °C, indicating thermal risks similar to those observed at 1.5T and 3T.

1. Introduction

Magnetic resonance imaging (MRI) at ultra‐high field (UHF) strengths has rapidly evolved over the past two decades, enabling unprecedented spatial resolution and image quality for human research.[1] With increasing field strength, MRI offers a higher signal-to-noise ratio (SNR), improved metabolic quantification, enhanced tissue contrast, and more efficient parallel imaging.[2], [3] Recently, the U.S. Food and Drug Administration (FDA) approved the clinical use of a 5T whole-body MRI system, marking a significant milestone in the transition of UHF MRI from research settings to clinical applications.

However, the shorter radiofrequency (RF) wavelengths and different field distributions at higher field strengths introduce unique safety concerns, particularly for patients with implantable medical devices.[4] One of the primary risks is localized tissue heating near metallic implants, caused by interactions between the RF fields and the implant structure, which can lead to resonance effects when the implant length approaches half the RF wavelength.

While extensive numerical and experimental studies have characterized RF-induced heating of orthopaedic metallic implants at 1.5T and 3T, and limited assessments exist for aneurysm clips and dental implants during 7T head MRI [5], [6], the RF safety of implants under 5T whole-body MRI remains largely unexplored. Among various devices, vascular stents are of particular interest because their length can be close to the resonant wavelength at 5T, potentially creating localized RF hotspots during scanning.

This study investigates RF-induced heating near stents of varying lengths placed in the right common carotid artery of an anatomically realistic human model during 5T MRI. The findings aim to provide foundational insights into local tissue heating near vascular stents, thereby informing future safety assessments and regulatory guidelines for the safe clinical use of 5T MRI in patients with vascular implants.

2. Methodology

The Specific Absorption Rate (SAR) quantifies the rate at which electromagnetic energy is absorbed by biological tissues during exposure to electromagnetic fields. It is closely linked to the temperature increase in tissues and is mathematically expressed as:

$$\mathrm{SAR(r)} = \frac{\sigma}{2\rho}\left|\vec{\mathrm{E}}(r)\right|^2 \propto \frac{\mathrm{dT}}{\mathrm{dt}} \tag{1}$$

where E is the total electric field at a given position (V/m), σ is the electrical conductivity (S/m), and ρ is the tissue density (kg/m³). In this study, electromagnetic simulations were conducted to evaluate the peak 1 g-averaged SAR near vascular stents under radiofrequency field exposure conditions relevant to 5T MRI.

Numerical electromagnetic simulations were

performed using Sim4Life (version 7.2, ZMT), a full-wave simulation software based on the Finite Difference Time Domain (FDTD) algorithm. The convergence criteria for all simulations were satisfied, with final convergence levels below –10 dB.

A generic eight-channel circularly polarized whole-body transmit coil (diameter: 60 cm; length: 45 cm) operating at 210.8 MHz was used to generate the incident electromagnetic field, representative of a 1.5 T MRI system. A radiofrequency shield (diameter: 64 cm; length: 150 cm) was included in the simulation environment to model realistic boundary conditions.

To accurately represent tissue interactions, two high-resolution anatomical human body models from the Virtual Population family were employed, as illustrated in Figure 1, with their key characteristics summarized in Table 1.

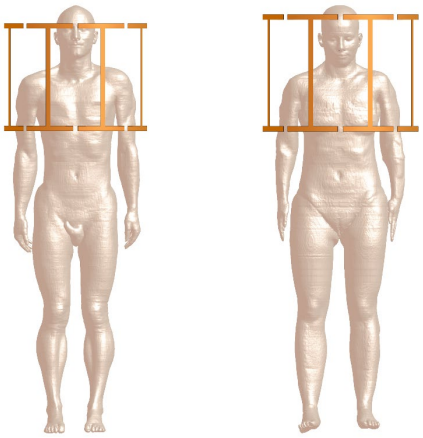

Figure 1. Illustration of the virtual human body model with birdcage coil: (A) Duke; (B) Ella.

Table 1. Information of the virtual human body models.

Information	Duke	Ella
Age (years)	34	26
Sex	Male	Female
Height (m)	1.77	1.63
Weight (kg)	70.2	57.3
BMI	22.4	21.6

These models include detailed anatomical structures such as major organs, vasculature, skeletal elements, and soft tissues. Dielectric properties of tissues were assigned based on the IT'IS Database v4.1 to ensure physiological accuracy.

As shown in Figure 2, vascular stents with lengths of 20, 30, 40, 50, and 60 mm and a diameter of 4 mm were modeled and positioned in the right common carotid artery, reflecting clinically relevant deployment sites.

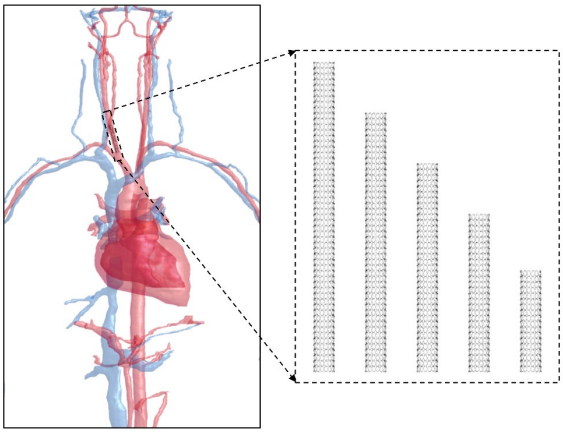

Figure 2. Stent placement illustration: the left panel shows the stent positioned inside the right common carotid artery, while the right panel displays stents of varying lengths (from left to right: 60, 50, 40, 30, and 20 mm).

Initially, the stent was placed at the isocenter (0 mm) of the RF coil. To evaluate the effect of imaging landmark position on RF exposure, the entire body model was shifted along the MRI bore axis by -200 mm, -100 mm, 100 mm, and 200 mm, respectively (Figure 3).

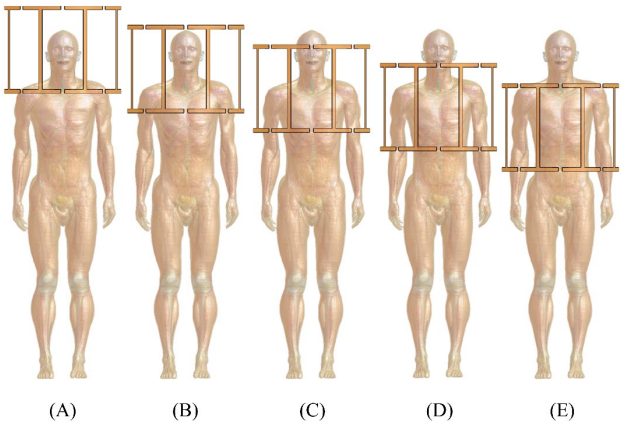

Figure 3. Imaging landmark illustration showing the human body shifted from left to right by −200, −100, 0, +100, and +200 mm.

SAR distributions were computed and normalized to comply with regulatory exposure limits: whole-body SAR of 2 W/kg and head SAR of 3.2 W/kg. Subsequently, temperature rise in the tissue surrounding the stents was estimated using Pennes' bioheat equation, which is implemented within Sim4Life. Simulations were run until a steady-state temperature distribution was reached, corresponding to 30 minutes of continuous RF exposure.

3. Result

3.1. Electric Field

Figure 4 illustrates the projection of the RMS magnitude of the electric field in the human body model on the coronal plane when a 6 cm stent is positioned at the isocenter of the RF coil. The electric field values are expressed in decibels, using 1500 V/m as the reference level.

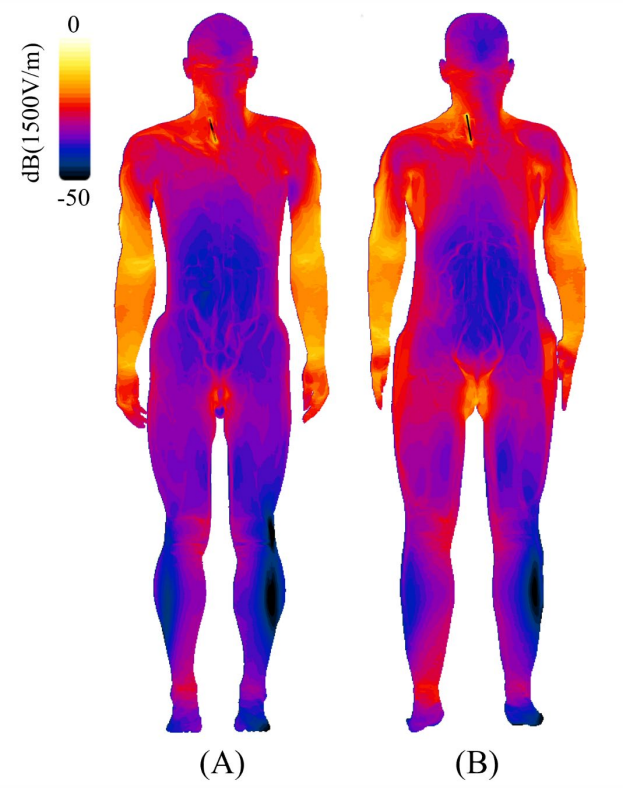

Figure 4. Coronal plane projection of the RMS magnitude of the electric field with a 6 cm stent at the RF coil isocenter: (A) Duke; (B) Ella.

It can be observed that, under this condition, the electric field is relatively strong in the chest region of the body model. In particular, a pronounced local enhancement of the electric field is observed in the region surrounding the stent.

3.2. 1g Weight-Averaged SAR

Figures 5 and 6 illustrate the peak SAR values in the vicinity of the stent for the Duke and Ella human models, respectively. The horizontal axis represents different loading positions, while the vertical axis indicates the peak 1 g weight-averaged SAR around the stent. Different curves correspond to different stent lengths.

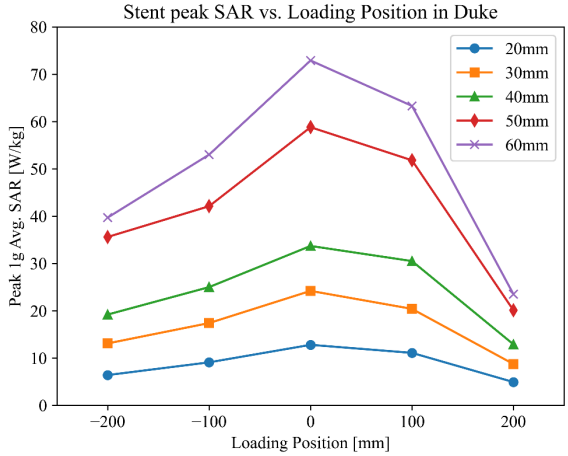

Figure 5. Peak SAR near the stent vs. loading position in Duke human body model.

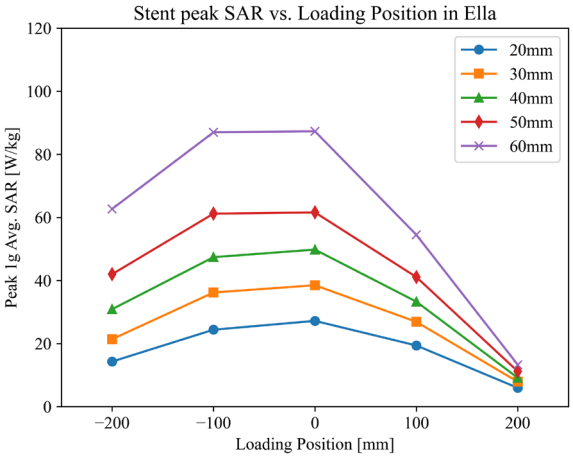

Figure 6. Peak SAR near the stent vs. loading position in Ella human body model.

It can be observed that the peak SAR reaches its maximum when the stent is positioned at the center of the RF coil. As the device is shifted toward either end of the coil, the peak SAR gradually decreases. For example, in the Duke model with a 60 mm stent, the peak SAR is 72.9 W/kg at the coil center, but drops to 23.5 W/kg when the stent is positioned at the lower end of the coil. A similar trend is observed in the Ella model.

The peak SAR also depends on the stent length: shorter stents produce less pronounced heating effects, whereas longer stents result in higher peak SAR values around the device. In the Duke model, as the stent length increases from 20 mm to 60 mm, the peak SAR rises from 12.8 W/kg to 72.9 W/kg. In the Ella model, the absolute values differ slightly from those in the Duke model but show the same overall pattern, increasing from 27.2 W/kg to 87.3 W/kg as the stent length increases.

3.3. Temperature Rise

For the Duke model in the worst-case scenario (60 mm stent, loading at the coil center), Figure 7(A) illustrates the SAR distribution around the stent. A region of elevated SAR can be observed in the vicinity of the stent, particularly concentrated at both ends of the device.

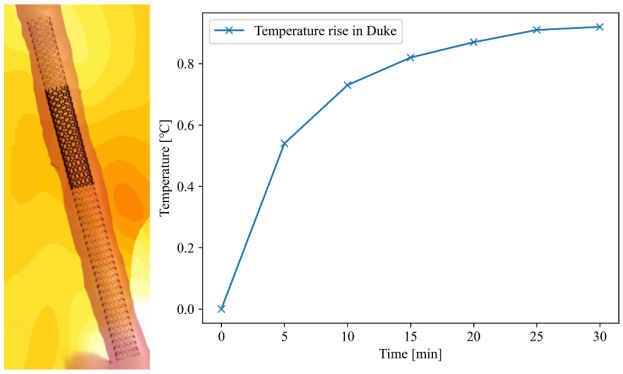

(A) (B)

Figure 7. Hot spot near the stent and its temperature rise: (A) SAR near the stent; (B) Hot spot temperature rise

Figure 7(B) presents the temperature rise at the hot spot. It can be seen that after 30 minutes of RF exposure, the temperature increase approaches a steady-state equilibrium, with the total temperature rise remaining below 1 °C.

4. Discussion

The variation of peak SAR with respect to the stent loading position is not strictly symmetric about the coil center. This asymmetry arises from the inherent anatomical asymmetry of the human body and is also related to the normalization scheme. When the stent is positioned near the lower edge of the coil, only the head and a small portion of the chest are located inside the coil. In this configuration, the transmitted power is limited by the head SAR of 3.2 W/kg, which allows relatively higher input power compared to other loading positions. As a result, the peak SAR at the lower edge is slightly higher than that near the upper edge.

Regarding the influence of stent length on SAR, elongated metallic implants can be approximated as linear antennas. When the implant length approaches half of the wavelength of the incident RF field in the surrounding medium, resonance occurs. This explains the increase in SAR values around the stent as its length increases, since the length gradually approaches the half-wavelength of the 5 T MRI RF coil (approximately 7 cm in tissue). At resonance length, the induced electric fields are enhanced, leading to higher local SAR values near the stent.

Despite the observed SAR distribution, the temperature rise around the stent remains relatively low. There are two main reasons for this. First, the stent has a small physical structure, with thin metallic wires forming its main body, resulting in limited heat generation. Second, the stent is located inside blood vessels, where blood perfusion plays a significant role. Although energy is deposited in the surrounding tissue, the generated heat is rapidly carried away by blood circulation, preventing significant temperature buildup.

5. Conclusion

This study demonstrates that stent length and positioning significantly influence SAR distribution and temperature rise, highlighting the importance of implant-specific MRI safety evaluations at 5 T. As ultra-high-field (UHF) MRI systems become more clinically viable, existing implant safety guidelines must be revised to account for the increased RF power deposition and wavelength-dependent resonance effects that occur at 5 T and higher field strengths.

References

[1] X. He *et al.*, "First in-vivo human imaging at 10.5T: Imaging the body at 447 MHz," *Magn. Reson. Med.*, vol. 84, no. 1, pp. 289–303, 2020, doi: 10.1002/mrm.28131.

[2] I. Tkáč, G. Öz, G. Adriany, K. Uğurbil, and R. Gruetter, "In vivo 1H NMR spectroscopy of the human brain at high magnetic fields: Metabolite quantification at 4T vs. 7T," *Magn. Reson. Med.*, vol. 62, no. 4, pp. 868–879, 2009, doi: 10.1002/mrm.22086.

[3] A. Abosch, E. Yacoub, K. Ugurbil, and N. Harel, "An Assessment of Current Brain Targets for Deep Brain Stimulation Surgery With Susceptibility-Weighted Imaging at 7 Tesla," *Neurosurgery*, vol. 67, no. 6, p. 1745, Dec. 2010, doi: 10.1227/NEU.0b013e3181f74105.

[4] L. Lan *et al.*, "Feasibility of cardiovascular magnetic resonance imaging at 5T in comparison to 3T," Oct. 25, 2022, *Research Square*. doi: 10.21203/rs.3.rs-2171514/v1.

[5] K. H. Salem, "Unreamed intramedullary nailing in distal tibial fractures," *Int. Orthop.*, vol. 37, no. 10, pp. 2009–2015, Oct. 2013, doi: 10.1007/s00264-013-1998-y.

[6] P. D. Hajek, H. R. J. Bicknell, W. E. Bronson, J. A. Albright, and S. Saha, "The use of one compared with two distal screws in the treatment of femoral shaft fractures with interlocking intramedullary nailing. A clinical and biomechanical analysis.," *JBJS*, vol. 75, no. 4, p. 519, Apr. 1993.

Address for correspondence:

Ji Chen.
Department of Electrical and Computer Engineering, University of Houston, Houston, TX 77204-4005, USA.
jchen23@Central.UH.EDU